Journal Pre-proof

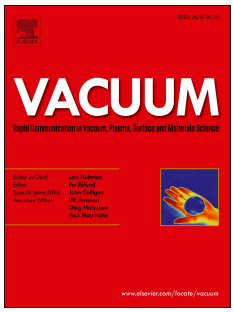

Facile synthesis OF CuCo2S4 nanoparticles as a faradaic electrode for high performance supercapacitor applications

M. Dakshana, S. Meyvel, M. Malarvizhi, P. Sathya, R. Ramesh, S. Prabhu, M. Silambarasan

PII: S0042-207X(20)30055-5

DOI: https://doi.org/10.1016/j.vacuum.2020.109218

Reference: VAC 109218

To appear in: *Vacuum*

Received Date: 27 September 2019

Revised Date: 17 January 2020

Accepted Date: 20 January 2020

Please cite this article as: Dakshana M, Meyvel S, Malarvizhi M, Sathya P, Ramesh R, Prabhu S, Silambarasan M, Facile synthesis OF CuCo2S4 nanoparticles as a faradaic electrode for high performance supercapacitor applications, *Vacuum*, https://doi.org/10.1016/j.vacuum.2020.109218.

FACILE SYNTHESIS OF $CuCo_2S_4$ NANOPARTICLES AS A FARADAIC ELECTRODE FOR HIGH PERFORMANCE SUPERCAPACITOR APPLICATIONS

M.Dakshana[a],S.Meyvel[a*],M.Malarvizhi[a], P.Sathya[b], R.Ramesh[c], S.Prabhu[c], M.Silambarasan[d]

[a]*Department of Physics, ChikkaiahNaicker College, Erode-638004, Tamilnadu ,India*

[b]*Department of Physics, Salem Sowdeswari College, Salem-636010, Tamilnadu, India*

[c]*Department of Physics, Periyar University, Salem – 636011, Tamilnadu, India*

[d]*Department of Physics, Vivekanandha College of Arts and Sciences for Women, Namakkal- 637205, Tamilnadu, India.*

***Corresponding author.**
E-mail address: meyvelphd@gmail.com (**S.MEYVEL**), **Mobile:** +91 9025459171.

ABSTARCT

In this paper, we report the synthesis of spinel $CuCo_2S_4$ nanoparticles (NPs) via a one-step hydrothermal method using two kinds of sulfur precursor's thioacetamide-TAA and thiourea-TU separately. The X-ray powder diffraction (XRD) analysis of both samples revealed a cubic phase of spinel $CuCo_2S_4$ crystal structure with Fd_3m space group. The spherical (19-20 nm) and hexagonal (17-19 nm) shaped NPs were observed by transmission electron microscope (TEM) images. N_2 adsorption-desorption results showed the high surface area of TAA-$CuCo_2S_4$ (91.03 m^2g^{-1}) than TU-$CuCo_2S_4$ (59.82m^2g^{-1}). XPS spectra exhibited the coexistence of Cu^{2+} and Cu^{3+} valence states of spinel cubic $CuCo_2S_4$. Electrochemical measurements showed that the TAA based $CuCo_2S_4$/Ni foam electrode has high specific capacity (1885 C g^{-1}/523 mA h g^{-1} at a current density of 2 Ag^{-1} about 5.4 times higher than thiourea based electrodes), ultrahigh capacity retention of 98% after 6000 GCD cycles at high current density of 10 Ag^{-1} and excellent energy density of 41.89 provided with a power density of 318.31W kg^{-1}.These results suggest that TAA assisted electrode material is suitable for improving electrochemical performance of supercapacitors.

Keywords: `

$CuCo_2S_4$; Hydrothermal method; non- capacitive type electrode; Specific capacity; Power density.

1. Introduction

With expedite devastation of fossil fuels and proliferating environmental pollution there is an imperative need for topical technologies bend with energy conversation and storage as well as clean, reversible, efficient and sustainable sources of energy [1]. Among various energy storage devices Rechargeable Supercapacitors(SCs) posses a high power density, long cycle life, high specific capacitance, very fast charging and discharging ability, and being cost-effective, environmentally friendly etc,. Owing to the above temperament, supercapacitors are pretend as a propitious candidate in energy storage and conversion [2-4]. Supercapacitors shows an extensive pertinence in military, transportation, consumer electronics, hybrid electrical vehicles, mobile communications, portable media players, back-up power supplies, pace makers and industrial machinery [2,5,6]. Hinge on, the charge storage execution supercapacitors are graded into two type's electrostatic or electric double layer capacitor [EDLC] and faradaic supercapacitor [FS] or pseudocapacitor.

In EDLC the electrode material is electrochemically inactive and the charges are physically accumulated between electrode and electrolyte interface. Hence, they provide a very low specific capacitance because the accessible active surface area decides the amount of charge to be stored. In Pseudocapacitor the electrode material is electrochemically active and the charges are stored by means of reversible faradaic reaction. Pseudocapacitor provides larger capacitance and energy density compared to EDLC, but still suffers from a low power density [1,2,7]. For the most part, supercapacitor chattels are swayed by framework of electrode material like specific surface area, pore size, pore distribution, electro active material, electrolyte and congregation technology [2,5]. Forthwith, electrode materials are studied in the view to recuperate the electrochemical pursuance for the extant materials and reinforcement of unfamiliar high performance electrode materials [2, 3].

Metal oxides/sulfides gathered tremendous attention in super capacitive electrodes due to its environmental affability, reasonable cost and high theoretical capacity. However, the experimental results do not provide satisfactory performance for practical applications. Therefore, countless works are concerned on building of electrode materials that posse a high specific capacitance. This leads to develop a capacitor with a high energy density that sustains a good scale capability under high charge – discharge current densities. Yet, there is a decrease in specific capacitance when current density increases due to the inappropriateness of electrolyte to the integral electrochemical active materials at the high current density, this also leads to the low areal specific capacitance which in turn forbids the practical applications. In order to overcome the above issues, electrode materials must meet the

following need, (i) rich redox reactions, which can manifest a high specific capacitance; (ii) high electrical conductivity which promotes fast electron transport; (iii) mesoporous and non destructive structure which provides a large amount of active sites for faradic redox reactions, fast ion diffusion and shorten the diffusion distance of electrolytes; (iv) binder free and non additives[8,9].

In the past decades, transition metal oxides/hydroxides (such as RuO_2, Mn_3O_4, Co_3O_4, NiO/Co $(OH)_2$, NiOH, NiFe double hydroxides [10,11]),carbon based materials (such as nanotubes, graphene, porous carbon etc. [10,12]), and conducting polymers and their derivatives (such as polypyrrole, polyaniline, etc.[12]) are more commonly on board to fabricate pseudocapacitors. In the case of transition metal oxides/hydroxides though they posses a high specific capacitance and good structure flexibility yet, still they suffer from low electron conductivity andthis could inhibit them from participating in commercial energy storage devices [13]. But, transition metal sulfides provide a high electrical conductivity, low cost, very high theoretical capacitance and lower band gap energy compared to transition metal oxides. Relate to binary transition metal sulfides (such as NiS, CoS, CoS_2, MoS_2, MnS, ZnS, CuS, etc.[11,14]), ternary transition metal sulfides (such as $NiCo_2S_4$, $CuCo_2S_4$, etc [13,15]) are mostly focused by researches due to its excellent electrochemical activity, higher specific capacitance gained by the participation of multiple cations during the surface redox reactions [11,12,13]. The lower electro negativity of sulfur than oxygen permits more flexible structure to protect weakening of structure through elongation between the layers and facilitates high electron transport potency in the structure. For the above reasons, transition metal sulfides attracted huge research attention as a promising electrode material for supercapacitors and Li-ion batteries [13, 15].

Thiospinels are spinel crystal structure commonly adopted by transition metal sulfides and posses a classic formula MM'_2S_4, where M and M´ are ordinarily divalent and trivalent metal cations. Single metal system are most commonly known thiospinels (M=M´) such as, Co_3S_4, Ni_3S_4, and Fe_3S_4. In Co_3S_4,some of the cobalt metalare exchanged with copper metal thatbring about a solid solution, conclusively forming the product $CuCo_2S_4$.$CuCo_2S_4$ is a mineral carrollite, with a normal spinel structure, in which Cu occupying the tetrahedral sites and Co occupying the octahedral sites [16,17]. Very recently, $CuCo_2S_4$ brand new ternary metal sulfide is utilized in fabrication of electrode material for application in energy storage device. Researchers have employed diverse techniques for the preparation of $CuCo_2S_4$nanoparticles such as microwave [18], hydrothermal [2,5,19], one- step sulphidation [20], solvothermal [21], oil bath [7], etc., In this present work, “hydrothermal method” was

carried out for the synthesis of $CuCo_2S_4$ nanoparticles. Advantages of adopting hydrothermal method are, it provides pure homogenous and well dispersed nanoparticles Owing to the fact that concurrent supply of high pressure and growth temperature to the mechanism operation of autoclave used in this technique. Moreover, this method provides control over parameters like time and the revolution per minute (rpm) on stirring this helps in achieving nanoparticles of desired shape and size [22,23].

Based on the above consideration, to the best of our knowledge for the very first time, we have fabricated $CuCo_2S_4$electrodes using two diverse sulfur sources and compared their electrochemical performance in a fruitful way. The as-obtained $CuCo_2S_4$ faradaic electrodes exhibits a significantly enhanced specific capacity of 348.86 C $g^{-1}$and 1885.49 C $g^{-1}$for thiourea and thioacetamide sulfur sources respectively and fine cyclic stability over 3000 cycles for thiourea based electrodes and 6000 cycles for thioacetamide based electrodes. The above features authenticates that the as-prepared $CuCo_2S_4$ faradaic electrodes are favourable for battery-type energy storage applications.

2. Experimental section

2.1. Materials

All Chemicals [Copper nitrate hexahydrate (Cu $(NO_3)_2 6H_2O$), Cobalt nitrate hexahydrate (Co $(NO_3)_2 6H_2O$), Thiourea ($SC(NH_2)_2$), Thioacetamide(C_2H_5NS) and ethanol] are purchased from Merk with analytical grade and are used without any further purification. Deionized (DI) water is utilized throughout the process.

2.2. Synthesis of $CuCo_2S_4$ Nanoparticles.

A facile One step hydrothermal method is adopted for preparing spinel $CuCo_2S_4$ nanoparticles with Thiourea (SC $(NH_2)_2$) [2] and Thioacetamide (C_2H_5NS) [13] sulfur sources discretely. In this archetypal procedure, at an ambient temperature 0.2mmol Cu $(NO_3)_2 6H_2O$ [6] and 0.4mmol Co $(NO_3)_2 6H_2O$ [6] got dissolved in 40ml deionized water by constant stirring for 30 minutes using a magnetic stir bar until a homogenous solution is achieved. Then, 0.8mmol SC $(NH_2)_2$ (sulfur source) got dissolved in 40 ml ethanol (solvent) and was added to the above concoction in a drop wise manner. The ending solution was transferred into a Teflon-lined stainless autoclave subsequent to 2 hours of stirring. The autoclave is sealed and heated to 160° for 12 hours then allowed to cool down naturally to room temperature. The obtained black precipitate was isolated via centrifugation (Hamilton Bell v6500 Vanguard centrifuge, 3000 RPM for 10 minutes) subsequently, rinsed thoroughly with deionized water and ethanol by a number of times to eradicate the residuals and was dried in a vacuum oven at 100°C for 7 hours to obtain $CuCo_2S_4$ nanoparticles (named as TU-

$CuCo_2S_4$).For comparison purposes, another $CuCo_2S_4$ product was also synthesized (named as TAA-$CuCo_2S_4$) under similar conditions using C_2H_5NS as sulfur source.

2.3. Structural, Morphological and Elemental characterization

The X-ray diffraction pattern of powder samples were taken by Philips XPERT-PRO diffractometer with graphite-monochromator using Cu Kα radiation at λ= 1.5418 Å, to identify the crystallographic nature and grain size of the synthesized products. TEM-Transmission electron microscope images with energy dispersive spectra (EDS) and their corresponding selected area electron diffraction (SAED) patterns were investigated through JEM-2100 (JEOL, JAPAN). XPS analyses were carried out on a KRATOS analytical spectrometer. The nitrogen adsorption-desorption techniques were performed using a BETSORP MAX (Microtrac BEL, Japan) to examine the surface area and porous nature of the sample.

2.4. Electrochemical Measurements

Electrode Preparation

Electrochemical measurements of $CuCo_2S_4$ were carried out to recognize redox properties using CHI 660E electrochemical workstation. All electrochemical parameters probed through a three electrode system with 2M KOH aqueous electrolyte solution at room temperature, sample loaded nickel foam as working electrode (WE), platinum as the counter electrode and Ag/AgCl as reference electrode. The working electrode was constructed by mixing the as-prepared sample, conductive carbon black and PVDF (Polyvinylidene Fluoride) at the mass ratio 80:15:5 followed by a suitable amount of NMP (N-Methyl-2-pyrolidone) and grinded to form a homogenous slurry. The ensuing slurry was crusted on the nickel foam (1x1 cm^2) and dried in oven under vacuum condition for 5hours at 80°C to get working electrode. The mass loading of electrode/cm^2 was tuned around 1.94mg/cm^2 for TU-$CuCo_2S_4$ and 1.81mg/cm^2 for TAA-$CuCo_2S_4$. Electrochemical impedance spectroscopy was also executed at this work station operated in at the frequency range of 100 KHz to 0.01Hz. A potential window in the range of 0.0 to 0.6 V was used throughout all electrochemical measurements

3. Results and Discussion

Nowadays, several research groups employ $CuCo_2S_4$ nanostructure for supercapacitor application. Among them, Wiltrout A. M. et al., have prepared $CuCo_2S_4$ nanoparticles by solution route based on two step process [17]. Mossavifard et al., reported a two-step solution based hydrothermal route for the synthesis of hierarchical $CuCo_2S_4$ nanostructures [24].

It is clear that all above mentioned synthesis methods required an elaborate process under hydrothermal condition this results in a time consuming and highly-priced for preparation of $CuCo_2S_4$ nanostructures. In order to overcome the above issue in this work, we have designed a simple one-step hydrothermal route method via ion- exchange reactions. This includes cation and anion exchange reactions and it is considered as an effective and low-cost method for chemical transformation of nanomaterials. Our work is followed by the anion-exchange reactions between s^{2-} and OH^- in hydrothermal environment. Hydrolyzation of thiourea is believed as the core mechanism which results in generation of alkaline environment (ammonia formation) and sulfide ions. The Cu^{2+} and Co^{2+} in the solution are co-precipitated to form Cu- Co hydroxides under the alkaline medium. The as precipitated hydroxides will be further converted to $CuCo_2S_4$ by reacting with S^{2-} via an ion- exchange process. The overall strategy is a combination of co-precipitation and sulfidation process into a single-step method making it a low-cost and time saving synthesis [25].

3.1. XRD Analysis

X-ray diffractogram of TU- $CuCo_2S_4$ (Fig.(1a)) firmly established a high intense and well crystallized narrow diffraction peaks positioned at 2θ= 26.6º,31.3º,38º,50º and 54.9º while TAA-$CuCo_2S_4$ (Fig.(1b)) mainly exhibit a low intense broad diffraction peaks situated at 2θ = 26.4º,31.3º,37.9º,49.9º and 54.7º. Both of the 2θ values showed the characteristic reflections of the cubic phase corresponding to (0 2 2), (1 1 3), (0 0 4), (1 1 5) and (0 4 4) planes of carrollite-type $CuCo_2S_4$ [21] (JCPDS card no. 42-1450) with Fd_3m space group [26]. The lattice constant of TAA-$CuCo_2S_4$ NPs is calculated as 9.543 Aº [26] which seems to be slightly higher than the lattice constant value (9.472 Aº) of TU-$CuCo_2S_4$.The non-existence of peaks from other crystallized phase signified the single phase $CuCo_2S_4$ with high purity. The crystallite size (D) was estimated from the Scherrer formula

$$D = K\lambda/\beta cos\theta \qquad (1)$$

Where, K is scherrer constant (commonly taken as 0.89),λ is the wavelength of the incident X- ray source (Cu Kα 0.15418 nm), β is the full width at half maximum and θ is the Braggs angle [27,28,22]. Rely on Debye-scherrer'sformula, the average grain size was found to be 20.39, 18.42 nm for TU-$CuCo_2S_4$, TAA-$CuCo_2S_4$ samples.

3.2. Morphological Analysis

TEM micrographs of TU-$CuCo_2S_4$ and TAA-$CuCo_2S_4$ is shown in Fig.2 (a, b) and Fig.3 (a, b) respectively. TU-$CuCo_2S_4$ indicated randomly orientated spherical like nanoparticles with a thick surface while TAA-$CuCo_2S_4$ exhibited approximately uniform hexagonal shaped nanoparticles. The average diameter of ununiform spherical nanoparticles

was found to be 19 to 20 nm and hexagonal nanoparticles are in the size range of 17 to19 nm which is in accord with grain size evaluated from XRD. As shown in Fig.2 (c), Fig.3 (c), the HRTEM images of TU-$CuCo_2S_4$ and TAA-$CuCo_2S_4$ clearly displayed (1 1 3), (1 1 1) planes of cubic $CuCo_2S_4$ that corresponds to lattice fringes with d-spacing value 0.28nm and 0.54nm.The equivalent well-ordered dark and light diffracting rings in Selected Area Electron Diffraction Patterns (SAED) of TU-$CuCo_2S_4$ (Fig.2d) and TAA-$CuCo_2S_4$ (Fig.3d) represent its polycrystalline characteristics. Variation in morphologies may be attributed to sulfur precursor of different origin. The presence of Cu, Co, S elements existed in the representative samples were confirmed EDS spectrum (Fig. (2e), Fig. (3e)). Furthermore, XPS characterization will be an authentication in verifying the purity of the prepared $CuCo_2S_4$.

3.3. XPS Measurements

X-Ray Photoelectron Spectroscopy (XPS) was conceded to enlighten about chemical states and surface elemental composition of $CuCo_2S_4$ nanoparticles.The typical XPS spectrum of TAA-$CuCo_2S_4$ given in Fig.4 (a) unveiled the presence of Cu, Co, and S elements. Manifestly, Cu 2p, Co 2p and S1s peaks are emerged out.

In the XPS analysis, binding energy (BE) referencing method is commonly performed with C 1s peak of adventitious carbon (AdC) to determine the chemical-state of specimens. Recent survey on XPS literature shows C 1s peak (E_B^F) position varied over a large range from 284.08 to 286.74 eV reliant on the substrate [29,30,31,32]. This situation is tackled by the consistent measurements and correlation $E_B^F + \varphi_{SA}$= constant (independent of material system used) suggested by Greczynski and Hultman [31,32]. It indicates invariant binding energy of the C1s peak in respect of the vacuum level.

The ultraviolet photoelectron spectroscopy (UPS) is employed to obtain the sample work function (WF) directly from the secondary electron cut-off using Helium lamp (attached to the XPS source) which provides the He I radiation with low energy of 21.2 eV and setting the C 1s peak of adventitious carbon at 289.58-φ_{SA}. Hence, the binding energy of C1s peak of AdC is set at 285.38 eV and all other core-levels are aligned accordingly.

Fig.4(b)involved Cu2p spectrum with two narrow peaks and two shake up satellite peaks. It showed the binding energies of Cu $2p_{3/2}$ and Cu $2p_{1/2}$ peaks at 933.3eV and 954.5eV, corresponding to the distinctive values of Cu^{2+} valence state with two satellite peaks (indicated as ‘sat’) at 943.2eV and 962.1eV [7].

As shown in Fig.4(c), the high resolution XPS spectrum of Co element comprised four peaks. Amid them, two strong peaks at 782.0e V and 796.6eV could be attributed to the existence of Co^{3+}, while the other two weak peaks at 778.9eV and 793.8eVcould be ascribed to Co^{2+}, which indicated the coexistence of Co^{3+} and Co^{2+} in the sample with spin-orbit splitting value (ΔE=15 eV) [33]. There might also exist a shakeup satellite peak at 803.1eV.This in turn provides abundant active sites for energy storage [15,3].

Fig.4 (d) labelled the XPS spectrum of S energy region. Two peaks at 161.3eV and 162.4eV were ascribed to $2p_{1/2}$ and $2p_{3/2}$core level of $S^{2-}$and the third peak at 169.3eV represented low coordination of sulphur ion (SO_4^{2-}) at the surface in $CuCo_2S_4$[34,35].The presence of SO_4^{2-}acknowledged that sulfur species on the sample's surface was partly oxidized in air. According to the results of XPS analysis, the near surface of the sample contained Co^{2+}, Co^{3+}, Cu^{2+} and S^{2-} [3,15]. These results are reliable with XRD and EDX analysis as mentioned above.

3.4. N_2 adsorption-desorption Analysis

Brunauer, Emmet, and Teller (BET) analysis of two$CuCo_2S_4$ samples (Fig.5 (a, b)) provide surface area evaluation based on nitrogen multilayer adsorption/desorption isotherms as a function of relative pressure. Consistently both adsorption/desorption curves showed a distinct Type IV isotherm with a characteristic hysteresis loop (H^3) which can be associated with a mesoporous (IUPUC, 2 nm<pore width <50 nm) structures [2, 36]. In addition to their analogous BJH analysis inset of Fig.5 (a,b), endorse the dubiety of mesoporous structure of the samples and their uniform pore size distributions curves are virtually confined in the optimal range of 2-5nm, which is examined as an ideal pore size range for electrochemical energy storage devices [15]. The obtained specific surface area of TAA-$CuCo_2S_4$ (91.03 m^2g^{-1}) is higher than TU-$CuCo_2S_4$ (59.82 m^2g^{-1}). Relatively, the mesoporous material with higher specific surface area contributes rich electro-active sites for faradic redox reactions and short diffusion paths to promote rapid electrolyte penetration, electrons transfer [37,19, 36,37].which results in ultra high rate capability, superior energy and power densities.[40] The above features such as surface area and pore diameters are reported as an aid in the advancement of electrochemical performance [41,42].

3.5. Electrochemical Properties

3.5.1. CV Analysis.

The cyclic voltammograms of TU-$CuCo_2S_4$ and TAA-$CuCo_2S_4$nanoparticleswith various scan rates 2.5, 5, 25, 50 and 100mV$s^{-1}$is displayed in Fig.6 (a) and Fig.7 (a).

Both CV curves depicted a quasi-rectangular shape. It revealed that the modified $CuCo_2S_4$ electrode has a novel battery type storage behaviour (i.e. coexistence of EDLC and battery like capacitive nature) originating from the faradaic process [43]. The obtained redox peaks are results of faradaic reactions upon Co^{2+}/Co^{3+} associated with OH anions. Furthermore, the relative intensified current response with increase in scan rate authenticates the speedy intercalation of electrons or ions within the electrode surface [7, 43]. The area under CV curve played a predominant role in defining the specific capacity of modified $CuCo_2S_4$ electrodes. The area of CV curves (at scan rate 2.5 mV s^{-1}) of representative electrodes is portrayed in Fig.6 (b) and Fig.7 (b). TAA-$CuCo_2S_4$ revealed a larger area compared to TU-$CuCo_2S_4$. It is noticeable that the larger the area under the curve, the larger the specific capacity of the electrode material, this can be further authenticated by resultant charge, discharge curves [19, 44].Furthermore, due to the over-potential and polarization effect of the electrode, the CV curves get slowly shifted from its quasi-rectangular shape during the linear increment in scan rate from 50 to 100mVs^{-1}[45].

3.5.2. Chronopotentiometric Analysis

In order to justify the characteristics of faradic non-capacitive electrode behaviour, the glavanostatic charge/discharge analysis were experimented. Fig.6(c) and Fig.7(c) illustrated the corresponding GCD curves of TU-$CuCo_2S_4$ and TAA-$CuCo_2S_4$ electrodes carried out at different current density from 2, 4, 6, 10 Ag^{-1}. Both electrodes exhibit a non linear charge/discharge curves, which comments as a characteristic of battery-type materials [7]. In other words, a rectangular CV with a triangular GCD is the essential EDLC behaviour. Aberration from the regular EDLC behaviour confirmed that the non linear charge/discharge curves were the upshot of diffusion controlled process viz the diffusion of the ions deep into the bulk electrode material. Owing to this fact, the energy storage mechanism is non-capacitive in nature. Hence, the amount of charge stored is approximately expressed in specific capacity (Cg^{-1} or $mAhg^{-1}$) rather than specific capacitance (Fg^{-1}), taking this into consideration the specific capacity (C_s) values Cg^{-1} of faradic non-capacitive type electrodes with a non linear charge/discharge curves are estimated using the equation (2) [43].

In order to compare the amount of charge stored with the previous literature, we have also calculated specific capacitance (F g^{-1}) using the formula (2a).This is employed for comparative purpose only.

$$C_s = \frac{1000 * i * t}{3600 * m} \qquad (2)$$

$$C_s = \frac{I\,\Delta t}{m\,\Delta V} \qquad (2a)$$

Where, i = current applied in ampere (A), t = discharge time in seconds (s), m= mass of the active material in gram (g), ΔV is operating voltage (V).

From non-linear charge/discharge curves, the specific capacity of modified TU-$CuCo_2S_4$ and TAA-$CuCo_2S_4$ electrodes at a current density of 2A g^{-1}, 4 A g^{-1}, 6 A g^{-1}, 10 A g^{-1} was computed as 348.86 C g^{-1} (96.90 m A h g^{-1} ; 242.26 F g^{-1}), 251.25 C g^{-1} (59.79 m A h g^{-1} ; 149.48 F g^{-1}), 122.47 C g^{-1} (34.02 m A h g^{-1} ; 85.05 F g^{-1}), 74.22 C g^{-1} (20.61 m A h g^{-1} ; 51.54 F g^{-1}) and 1885.49 C g^{-1} (523.75 m A h g^{-1} ; 1309.39 F g^{-1}), 1805.96 C g^{-1} (501.65 m A h g^{-1} ; 1254.14 F g^{-1}), 1515.58 C g^{-1}(420.99 m A h g^{-1}; 1052.48 F g^{-1}), 1451.93 C g^{-1}(403.31 m A h g^{-1} ; 1008.28 F g^{-1}). The specific capacity of TAA-$CuCo_2S_4$ is found to be approximately 5.4 fold higher than the specific capacity of TU-$CuCo_2S_4$.The plot of current density Vs specific capacity (Fig.8) clearly indicates the decrease of specific capacity with the increase of current density. The inadequate utilization of electro – active material [45], controlled diffusion, existence of inner active sites and transfer of OH^- ion in the electrolyte[46] and the effect of increment of voltage drop [45] factors are highly concerned in redox reaction at high current densities, they are incompetent to support the redox transitions completely[46].The highest specific capacity is achieved by the high specific surface area [42] this facilities the reversible faradaic reactions by providing more electrochemical active sites and the porous nanostructures of both TAA-$CuCo_2S_4$ and TU-$CuCo_2S_4$ served as ion-buffering reservoirs that provide efficient faradaic reactions for energy storage by maintaining the sustenance of the electrolyte ions [46]. The obtained specific capacity values are found to be far superior compared to the previously reported values as summarized in Table.1.

3.5.3. Cycleability test.

To evaluate the cyclic stability of both samples, their corresponding electrodes are put into continues charge/discharge cycles of 6000 cycles at a high current density of 10A g^{-1}as shown in Fig.9. Notably, TAA-$CuCo_2S_4$ exhibits superior cyclic stability of complete 6000

cycles while TU-$CuCo_2S_4$ disclose 3000 cycles only.TAA-$CuCo_2S_4$ electrode shows the ultra-high capacitance retention of 98% after 6000 successive GCD cycles, while TU-$CuCo_2S_4$ electrode dropped at 82 % after 3000 GCD cycles. This evinced the complete activation process of active material TAA-$CuCo_2S_4$ over 6000 cycles. Since, structural stability of the electrode material plays a vital role in maintaining the cyclic stability [47] TU-$CuCo_2S_4$ electrode expressed reduced cycles due to the effect of interaggregated nanoparticles which are not suitable for the long term redox reactions.

Practical applications of TAA-$CuCo_2S_4$ and TU-$CuCo_2S_4$ mainly depend on energy and power density that can be analyzed by Ragone plot (Fig.10). Therefore, the energy density and power density are calculated from the GCD curves for different current densities based on the given equation (3) and equation (4) [48,49].

$$\text{Energy density} \qquad E = \frac{1}{2} C_{sp} \Delta V^2 \qquad (3)$$

$$\text{Power density} \qquad P = \frac{E}{\Delta t} \qquad (4)$$

Where, E is energy density (W h kg^{-1}), P is power density (W kg^{-1}), C_{sp} is specific capacity (C g^{-1}), ΔV is operating voltage (V) and Δt is discharge time (s).

TAA-$CuCo_2S_4$ offers a very high energy density of 41.89W h kg^{-1} with a suitable power density of 318.31 W kg^{-1}. Even at a high power density of 1591.51 Wkg^{-1} it still maintains to deliver an energy density of 32.26 (W h kg^{-1}). These values are found to be slightly higher than the previously reported energy and power density values by Yuqiao Wang et al., [4].

3.5.4. EIS Analysis.

EIS measurements were carried out in determining impedance response of TAA-$CuCo_2S_4$andTU-$CuCo_2S_4$ electrode materials in the frequency range 0.01Hz to 100 kHz at an open-circuit potential of amplitude 5mV. Nyquist plot (Fig.11) is utilized to explicate electrochemical behaviour, rate capability etc., It is a collection of two sections, a semicircle in the high frequency range and a linear line in the low frequency range. The intercept of semicircle on the real axis relates to the internal resistance (R_s) and the diameter of the semicircle illustrates the Charge transfer resistance (R_{ct}) of faradaic process [14]. It is clearly evident that compare to TU-$CuCo_2S_4$ (1.12 Ω) electrode, TAA-$CuCo_2S_4$ (0.53 Ω) electrode reveal a very low internal resistance (R_s).Furthermore, EIS curve of TAA-$CuCo_2S_4$ electrode reveals a smaller semicircle compare to TU-$CuCo_2S_4$ electrode. In addition, TAA-$CuCo_2S_4$

shows more ideal vertical line compare to TU-$CuCo_2S_4$, suggesting efficient electrolyte and good diffusion rate of protons [50].

4. Conclusion

In summary, a facile one step hydrothermal method has been implemented to synthesize spinel $CuCo_2S_4$ nanoparticles using thiourea and thioacetamide sulfur sources. XRD patterns revealed a formation of well-crystalline $CuCo_2S_4$ nanoparticles with cubic spinel structure.TEM images showed hexagonal shape of nanoparticles in the range 17 - 19 nm. XPS analysis acknowledged the co-existence of Co^{2+} and Co^{3+} valence state in TAA-$CuCo_2S_4$. BET studies provided a high surface area of 91.03 m^2g^{-1} and an optimal pore size distribution (2-5nm). The structural, morphological and electrochemical performance suggests that thioacetamide assisted $CuCo_2S_4$ (TAA) nanoparticles are suitable material for high performance (battery-type) supercapacitor applications with excellent specific capacity of 1885.49 C g^{-1}/523.75 mA h g^{-1} at a current density of 2 Ag^{-1} and also a superior capacity retention of 98% even after 6000 GCD cycles at a high current density of 10Ag^{-1} endowed with a high energy density of 41.89 W h kg^{-1} with a suitable power density of 318.31(Wkg^{-1}). Our work plays an initiative role in designing other types of ternary metal sulfides as faradaic electrode with high energy storage.

Reference:

[1]. Guoping Wang, Lei Zhang, and Jiujun Zhang, A Review of Electrode Materials For Electrochemical Supercapacitors, Chem. Soc. Rev, 41 (2012) 797-828.

[2].Yirong Zhu, XiaoboJi, Han Chen, Liujiang Xi, Wenqiang Gong, and Yong Liu, The Investigation of the Electrochemically Supercapacitive Performances of Mesoporous$CuCo_2S_4$,RSC Adv, 6 (2016) 84236-41.

[3]. Qiufan Wang, Xiao Liang, Depeng Yang, and Daohong Zhang, Facile Synthesis of Novel $CuCo_2S_4$Nanospheres for Coaxial FiberSupercapacitors, RSC Adv, 7 (2017) 29933-37.

[4]. Yuqiao Wang, Dawei Yang, Tianyue Zhou, JiePan, Tao Wei, and Yueming Sun, Oriented $CuCo_2S_4$Nanograss Arrays/Ni Foam as an Electrode for a High-Performance All-Solid-State Supercapacitor, Nanotech, 28 (2017) 465402.

[5]. Haihua Hu, Jiqiu Qi, Yanwei Sui, Yaoyao Zhou, Fuxiang Wei, Yezeng He, QingkunMeng, Zhi Sun, Guoqing Zhang, and Ziping Wang, Facile Synthesis of Copper Sulfides with Different Shapes for High-Performance Supercapacitors, J. Mater.Sci: Mater Electron, 28 (2017) 10720-29.

[6]. Young Hun Lee, Bong Kyun Kang, Min Seob Kim, HyungWook Choi, Dong Soo Choi,Mohit Kumar, and DaeHo Yoon, Synthesis and Characterization of Highly Uniform $CuCo_2S_4$ Ball-in-Ball Hollow Nanospheres as High Performance Electrode for Supercapacitors, Phys. Status Solidi (a),215 (2018) 1700936.

[7].M.Silambarasan, N.Padmanathan, P.S.Ramesh, and D.Geetha, Spinel$CuCo_2O_4$Nanoparticles: Facile One-Step Synthesis, Optical, and Electrochemical Properties, Mater. Res.Express,3 (2016) 095021.

[8]. Jialin Yin, Hao Zhang, JiaqiuLuo, Mengqi Yao, and Wencheng Hu, High-Boiling-Point Solvent Synthesis of Mesoporous $NiCo_2S_4$with High Specific Surface Area as Supercapacitor Electrode Material, J. Mater.Sci: Mater Electron, 28 (2017) 2093-99

[9]. X.F.Gong, J.P.Cheng, K.Y.Ma, F.Liu, LiZhang, and XiaoBin Zhang, Nanostructured Nickel-Cobalt Sulfide Grown on Nickel Foam Directly as Supercapacitor Electrodes with High Specific Capacitance, Mater. Chem. Phys,173 (2016) 317-24.

[10]. Ping Wen, Mingjin Fan, Desuo Yang, Yan Wang, Hualei Cheng, and Jinqing Wang, An Asymmetric Supercapacitor with Ultrahigh Energy Density Based on Nickle Cobalt

SulfideNanocluster Anchoring Multi-Wall Carbon Nanotubes Hybrid, J. Power Sources, 320 (2016) 28-36.

[11]. LemuGirmaBeka, Xin Li, Xianjun Xia, and Weihua Liu, 3D Flower-Like $CoNi_2S_4$Grown on Graphene Decorated Nickel Foam as High Performance Supercapacitor,Diam. Relat. Mater,73 (2017) 169-76.

[12]. Yang Lu, Zongwen Zhang, Xianming Liu, Weixiao Wang, Tao Peng, PengfeiGuo, Haibin Sun, Hailong Yan, and YongsongLuo, $NiCo_2S_4$/Carbon Nanotube Nanocomposites with a Chain-Like Architecture for Enhanced Supercapacitor Performance, Cryst.Eng.Comm, 18 (2016) 7696-706.

[13]. Siyi Cheng, Tielin Shi, Chen Chen, Yan Zhong, Yuanyuan Huang, Xiangxu Tao, Junjie Li, Guanglan Liao, and Zirong Tang,Construction of Porous $CuCo_2S_4$Nanorod Arrays Via Anion Exchange for High-Performance Asymmetric Supercapacitor, Sci. Rep., 7 (2017) 6681.

[14]. Jun Pu, Tingting Wang, Haiyang Wang, Yao Tong, Chenchen Lu, Wei Kong, and Zhenghua Wang, Direct Growth of $NiCo_2S_4$ Nanotube Arrays on Nickel Foam as High-Performance Binder-Free Electrodes for Supercapacitors, ChemPlusChem, 79 (2014) 577-83.

[15]. Delong Li,Youning Gong, and Chunxu Pan, Facile Synthesis of Hybrid CNTs/$NiCo_2S_4$Composite for High Performance Supercapacitors, Sci. Rep, 6 (2016) 29788.

[16]. RoghayehHashemiFath, and S JafarHoseini, Synthesis of Thiospinel $CuCo_2S_4$ and $CuCo_2S_4$/Reduced-Graphene Oxide Nanohybrids as Highly Effective Catalysts for the SonogashiraReaction,New J Chem, 41 (2017) 3392-98.

[17]. Alex M Wiltrout, Carlos G Read, Evan M Spencer, and Raymond E Schaak, Solution Synthesis of Thiospinel$CuCo_2S_4$ Nanoparticles, Inorg.chem, 55 (2015) 221-26.

[18]. Li Gu, Lei Qian, Ying Lei, Yanyan Wang, Jing Li, Hongyan Yuan, and Dan Xiao, , Microwave-Assisted Synthesis of Nanosphere-Like $NiCo_2O_4$ Consisting of Porous Nanosheets and Its Application in Electro-Catalytic Oxidation of Methanol, J.Power Sources, 261(2014) 317-23.

[19]. Yirong Zhu, Xianhong Chen, Wei Zhou, KaixiongXiang, Weida Hu, and Han Chen, , Controllable Preparation of Highly Uniform $CuCo_2S_4$ Materials as Battery Electrode for Energy Storage with Enhanced Electrochemical Performances, Electrochim. Acta, 249(2017) 64-71.

[20]. Haihua Hu, Yanwei Sui, Yaoyao Zhou, Jiqiu Qi, Fuxiang Wei, Yezeng He, QingkunMeng, Zhi Sun, and Yulong Zhao, One-Pot Synthesis of Flake $Cu_{1.81}S$/C Composite for High-Performance Supercapactiors Electrodes, Micro & Nano Letters, 12 (2017) 87-89.

[21]. L Nie, H Wang, S Liu, and R Yuan, Solvothermal Synthesis of $CuCo_2S_4$ Nanoparticles for Rechargeable Lithium-Ion Battery Anodes, Chalcogenide Lett, 13 (2016) 555-62.

[22]. Davoud Dastan, Effect of Preparation Methods on the Properties of Titania Nanoparticles: SolvothermalVersus Sol–Gel, Appl. Phys.A, 123 (2017) 699.

[23]. Davoud Dastan, and Arun Banpurkar, Solution Processable Sol–Gel Derived Titania Gate Dielectric for Organic Field Effect Transistors, J. Mater. Sci: Mater Electron, 28 (2017) 3851-59.

[24]. Moosavifard, Seyyed Ebrahim, Fani Saeed and Rahmanian Mehdi. Hierarchical $CuCo_2S_4$ hollow nanoneedle arrays as novel binder-free electrodes for high-performance asymmetric supercapacitors , Chem. Commun, 52 (2016) 4517-4520.

[25]. Verma, Rakesh, Kothandaraman, R and Varadaraju, UV. In-situ carbon coated CuCo2S4 anode material for Li-ion battery applications Appl. Surf. Sci, 418 (2017) 30-39

[26]. Zhen Tian, Xiaomin Wang, BoxiaLi, Huijun Li, and Yucheng Wu, High Rate Capability Electrode Constructed by Anchoring Cuco2s4 on Graphene Aerogel Skeleton toward Quasi-Solid-State Supercapacitor, Electrochimica Acta, 298 (2019) 321-29.

[27].Davoud Dastan, and NB Chaure, Influence of Surfactants on TiO_2 Nanoparticles Grown by Sol-Gel Technique. Int.J.Mater.Mech. Manuf ,2 (2014) 21-24.

[28]. Davoud Dastan, Priyanka U Londhe, and Nandu B Chaure, Characterization of TiO_2 Nanoparticles Prepared Using Different Surfactants by Sol–Gel Method, J. Mater. SciMater.Electron, 25 (2014) 3473-79.

[29]. T.L. Barr, S.Seal, Nature of the use of adventitious carbon as a binding energy standard J.Vac.Sci.Technol.A 13 (1995) 1239.

[30]. S.H.Lee, E.Yamasue, K.N.Ishihara,H.Okumara, Photocatalysis and surface doping states of N-doped TiO_x films prepared by reactive sputtering with dry air Appl.Catalysis B: Environ. 93 (2010) 217.

[31]. G. Greczynski, L. Hultman, X-ray photoelectron spectroscopy: Towards reliable binding energy referencing, Prog. Mater. Sci, 107 (2019) 100591.

[32]. Greczynski G, Hultman L. Reliable determination of chemical state in x-ray photoelectron spectroscopy based on sample-work-function referencing to adventitious carbon: resolving the myth of apparent constant binding energy of the C 1s peak., Appl Surf Sci., 451 (2018) 99-103.

[33]. MeenakshiChauhan, KasalaPrabhakar Reddy, Chinnakonda S Gopinath, and SasankaDeka, Copper Cobalt SulfideNanosheets Realizing a Promising Electrocatalytic Oxygen Evolution Reaction, ACS Cata, 7 (2017) 5871-79.

[34]. CaihongFeng, Le Zhang, Menghuan Yang, Xiangyun Song, Hui Zhao, ZheJia, Kening Sun, and Gao Liu, One-Pot Synthesis of Copper Sulfide Nanowires/Reduced Graphene Oxide Nanocomposites with Excellent Lithium-Storage Properties as Anode Materials for Lithium-Ion Batteries, Appl.Mater. Interfaces, 7 (2015) 15726-34.

[35]. Liang-Liang Feng, Guo-Dong Li, Yipu Liu, Yuanyuan Wu, Hui Chen, Yun Wang, Yong-CunZou, Dejun Wang, and XiaoxinZou, Carbon-ArmoredCo_9S_8 Nanoparticles as All-Ph Efficient and Durable H2-Evolving Electrocatalysts, ACS Appl. Mater. Interfaces, 7 (2015) 980-88.

[36]. Y.M. Zhang, Y.W. Sui, J.Q. Qi, P.H.Hou, F.X. Wei, Y.Z. He, Q.K.Meng, and Z.Sun, Facile Synthesis of $NiCo_2S_4$Spheres with Granular Core Used as Supercapacitor Electrode Materials, J.Mater. Sci: Mater Electron,28 (2017) 5686-95.

[37]. Bing Guan, Yu Li, Biyue Yin, Kefan Liu, Dawei Wang, Huaihao Zhang, and Changjing Cheng, Synthesis of Hierarchical NiS Microflowers for High Performance Asymmetric Supercapacitor,ChemEng.J. ,308 (2017) 1165-73.

[38]. Balamurugan, Jayaraman, Nguyen, Thanh Tuan, Aravindan, Vanchiappan, Kim, Nam Hoon and Lee, Joong Hee. Flexible Solid-State Asymmetric Supercapacitors Based on Nitrogen-Doped Graphene Encapsulated Ternary Metal-Nitrides with Ultralong Cycle Life. Adv. Funct. Mater, *28* (2018), 1804663.

[39]. Nguyen, Thanh Tuan, Balamurugan, Jayaraman, Aravindan, Vanchiappan, Kim, Nam Hoon and Lee, Joong Hee. Boosting the Energy Density of Flexible Solid-State Supercapacitors via Both Ternary NiV_2Se_4 and $NiFe_2Se_4$ Nanosheet Arrays. Chem mater. (2019).

[40]. Balamurugan Jayaraman, Li Chao Aravindan, Vanchiappan Kim Nam Hoon and Lee, Joong Hee. Hierarchical Ni · Mo · S and Ni · Fe · S Nanosheets with Ultrahigh Energy Density for Flexible All Solid-State Supercapacitors. Adv. Funct. Mater 28

(2018), 1803287.

[41]. DavoudDastan, NanduChaure, and Moses Kartha, Surfactants Assisted Solvothermal Derived Titania Nanoparticles: Synthesis and Simulation,J. Mater. SciMater.Electron, 28 (2017) 7784-96.

[42]. Balamurugan Jayaraman, Nguyen Thanh Tuan, Aravindan Vanchiappan, Kim Nam Hoon, Lee Seung Hee and Lee, Joong Hee. All ternary metal selenide nanostructures for high energy flexible charge storage devices. Nano Energy 65 (2019) 103999.

[43]. AtinPramanik, SandipanMaiti, MonjoySreemany, and SourindraMahanty, Carbon Doped $MnCo_2S_4$ Microcubes Grown on Ni Foam as High Energy Density Faradaic Electrode, Electrochim. Acta, 213 (2016) 672-679.

[44]. Nguyen Thanh Tuan, Balamurugan Jayaraman, Kim Nam Hoon and Lee Joong He. Hierarchical 3D Zn–Ni–P nanosheet arrays as an advanced electrode for high-performance all-solid-state asymmetric supercapacitors. J. Mater Chem A 6 (2018) 8669-8681.

[45]. M Silambarasan, PS Ramesh, D Geetha, and V Venkatachalam, A Report on 1D $MgCo_2O_4$ with Enhanced Structural, Morphological and Electrochemical Properties, J. Mater.Sci: Mater Electron,28 (2017) 6880-88.

[46]. Tao Zhu, Guoxiong Zhang, Tao Hu, Zhenni He, Yisheng Lu, Guiqing Wang, HaiboGuo, JianLuo, Chuan Lin, and Yigang Chen, Synthesis of $NiCo_2S_4$-Based Nanostructured Electrodes Supported on Nickel Foams with Superior Electrochemical Performance, J. Mater. Sci,51 (2016) 1903-13.

[47].Jianhua Tang, YuancaiGe, JianfengShen, and MingxinYe, Facile Synthesis of $CuCo_2S_4$ as a Novel Electrode Material for Ultrahigh Supercapacitor Performance, ChemComm, 52 (2016) 1509-12.

[48]. Ghosh, Debasis, Giri, Soumen and Das, Chapal Kumar Preparation of CTAB-assisted hexagonal platelet Co (OH) 2/graphene hybrid composite as efficient supercapacitor electrode material. ACS Sustainable Chemistry & Engineering 1 (2013) 1135-1142.

[49]. Zhang, Jinglin, Liu, Huidi, Shi, Pu, Li, Yaoji, Huang, Langhuan, Mai, Wenjie, Tan, Shaozao and Cai, Xiang. Growth of nickel (111) plane: The key role in nickel for Further improving the electrochemical property of hexagonal nickel hydroxide-nickel & reduced graphene oxide composite. J. Power Sources. 267 (2014) 356-365.

[50] .R BoopathiRaja, M Parthibavarman, and A Nishara Begum, Hydrothermal Induced Novel CuCo2o4 Electrode for High Performance Supercapacitor Applications, Vacuum, 165, (2019) 96-104.

[51]. Young Hun Lee, Bong Kyun Kang, Min Seob Kim, HyungWook Choi, Dong Soo Choi,Mohit Kumar, and DaeHo Yoon, Synthesis and Characterization of Highly Uniform $CuCo_2S_4$ Ball-in-Ball Hollow Nanospheres as High Performance Electrode for Supercapacitors, Phys. status solidi (A), 215 (2018) 1700936.

[52]. KP Annamalai, and You-sheng Tao, A Hierarchically Porous $CuCo_2S_4$/Graphene Composite as an Electrode Material for Supercapacitors, New Carbon Mater, 31 (2016) 336-42.

Figure Captions

Fig.1. XRD Analysis.Comparison between X-ray diffraction patterns of **(a)** $CuCo_2S_4$ using thiourea **(b)** $CuCo_2S_4$ using thioacetamide.

Fig.2.TEM IMAGES.**(a,b)** TEM images of synthesized TU-$CuCo_2S_4$ nanoparticles, **(c)**HRTEM image of TU- $CuCo_2S_4$ **(d)**SAED patterns of TU- $CuCo_2S_4$ and **(e)** EDAX spectrum of TU- $CuCo_2S_4$.

Fig.3.TEM IMAGES.**(a,b)** TEM images of synthesized TAA-$CuCo_2S_4$ nanoparticles, **(c)**HRTEM image of TAA- $CuCo_2S_4$ **(d)**SAED patterns of TAA- $CuCo_2S_4$ and**(e)** EDAX spectrum of TAA- $CuCo_2S_4$

Fig.4. XPS ANALYSIS.**(a)**A typical survey XPS spectrum, and high resolution XPS spectra of **(b)** Cu**(c)** Co and **(d)** S elements of the as-prepared TAA-$CuCo_2S_4$ nanoparticles.

Fig.5. N_2 sorption isotherms and Differential mesopore size distribution $\Delta V/\Delta d$ plots (inset) of (**a)** TU-$CuCo_2S_4$ and **(b)** TAA-$CuCo_2S_4$

Fig.6. Electrochemical characterization of TU-$CuCo_2S_4$ modified electrode, **(a)** CV curves of TU-$CuCo_2S_4$ at varying scan rates, **(b)** area under the curve for a scan rate of 2.5mVs^{-1}, **(c)** charge- discharge curves of TU-$CuCo_2S_4$at dissimilar current densities

Fig.7. Electrochemical characterization of TAA-$CuCo_2S_4$ modified electrode, **(a)** CV curves of TAA- $CuCo_2S_4$ at various scan rates, **(b)** area under the curve for a scan rate of 2.5mVs^{-1}, **(c)** charge-discharge curves of TAA- $CuCo_2S_4$ at various current densities

Fig.8. Current density Vs specific capacity plot

Fig.9. Cyclic stability of the prepared $CuCo_2S_4$ electrodes for 6000 cycles at high current density of 10 A g^{-1}.

Fig.10. Ragone Plot of the prepared TU-$CuCo_2S_4$, TAA-$CuCo_2S_4$ samples

Fig.11. EIS plot of TU-$CuCo_2S_4$, TAA-$CuCo_2S_4$ electrodes.

Table Captions

Table.1. Comparison of specific capacity / specific capacitance for synthesized sample with other reported electrode materials.

Table 1

Electrode Materials	**Synthesis route**	**Current Density**	**Specific Capacity/Specific Capacitance**	**Number of cycles**	**Reference**
$CuCo_2S_4$ (TAA)	Hydrothermal method	2 A g^{-1}	**1309.39 F g^{-1} ; (523.75 m A h g^{-1})**	**6000**	**This work (TAA-$CuCo_2S_4$)**
$CuCo_2S_4$	Hydrothermal method	2 A g^{-1}	752 F g^{-1}	5000	[2]
$CuCo_2S_4$	Hydrothermal method	0.5 A g^{-1}	442 F g^{-1}	5000	[51]
$CuCo_2S_4$	Hydrothermal method	2 A g^{-1}	90.6 mAh g^{-1}	5000	[19]
$CuCo_2S_4$	Hydrothermal method	1 A g^{-1}	525 F g^{-1}	1000	[52]

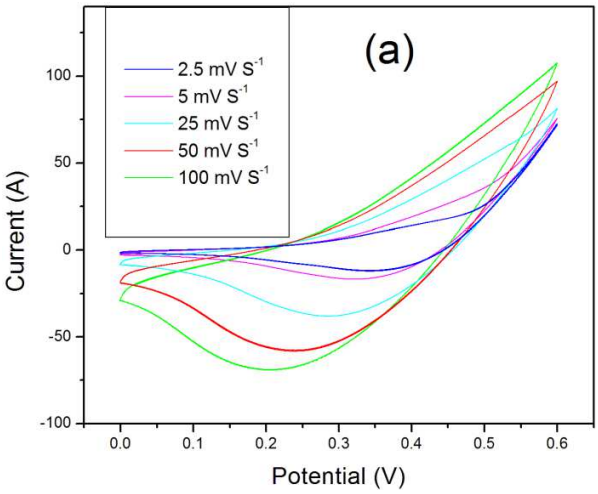
(a)
2.5 mV S-1
5 mV S-1
25 mV S-1
50 mV S-1
100 mV S-1
Current (A)
Potential (V)

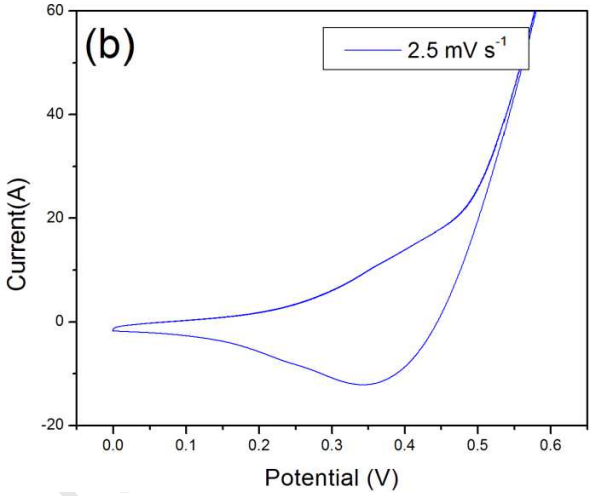
(b)
2.5 mV s-1
Current(A)
Potential (V)

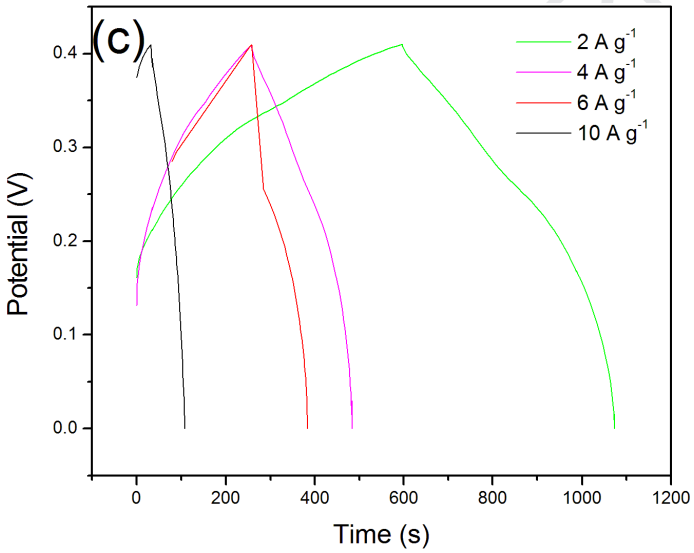
(c)
2 A g-1
4 A g-1
6 A g-1
10 A g-1
Potential (V)
Time (s)

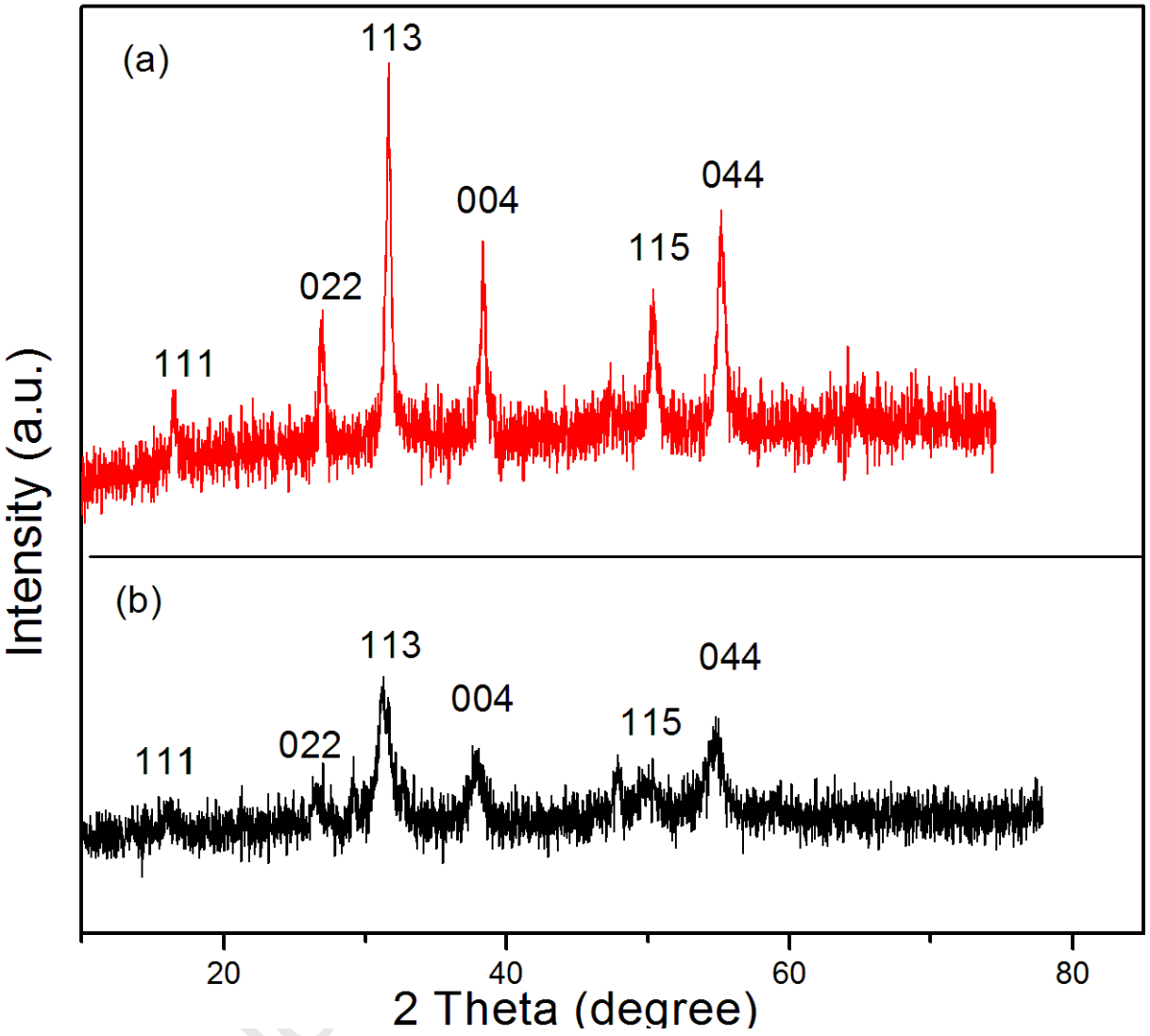
(a)
113
044
004
115
022
111
(b)
113
044
004
115
022
111
Intensity (a.u.)
20
40
60
80
2 Theta (degree)

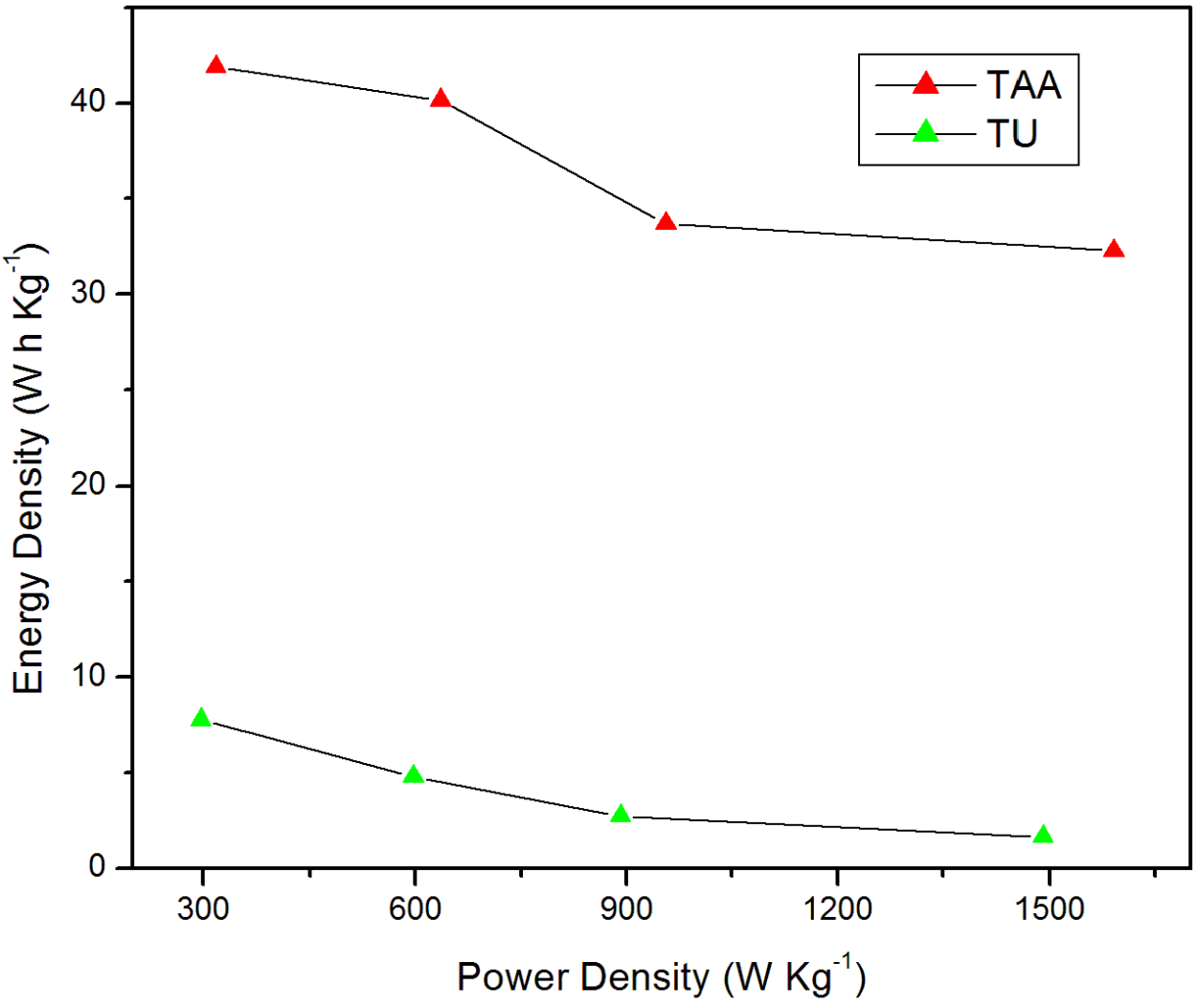
TAA
TU
Energy Density (W h Kg-1)
Power Density (W Kg-1)
0
10
20
30
40
300
600
900
1200
1500

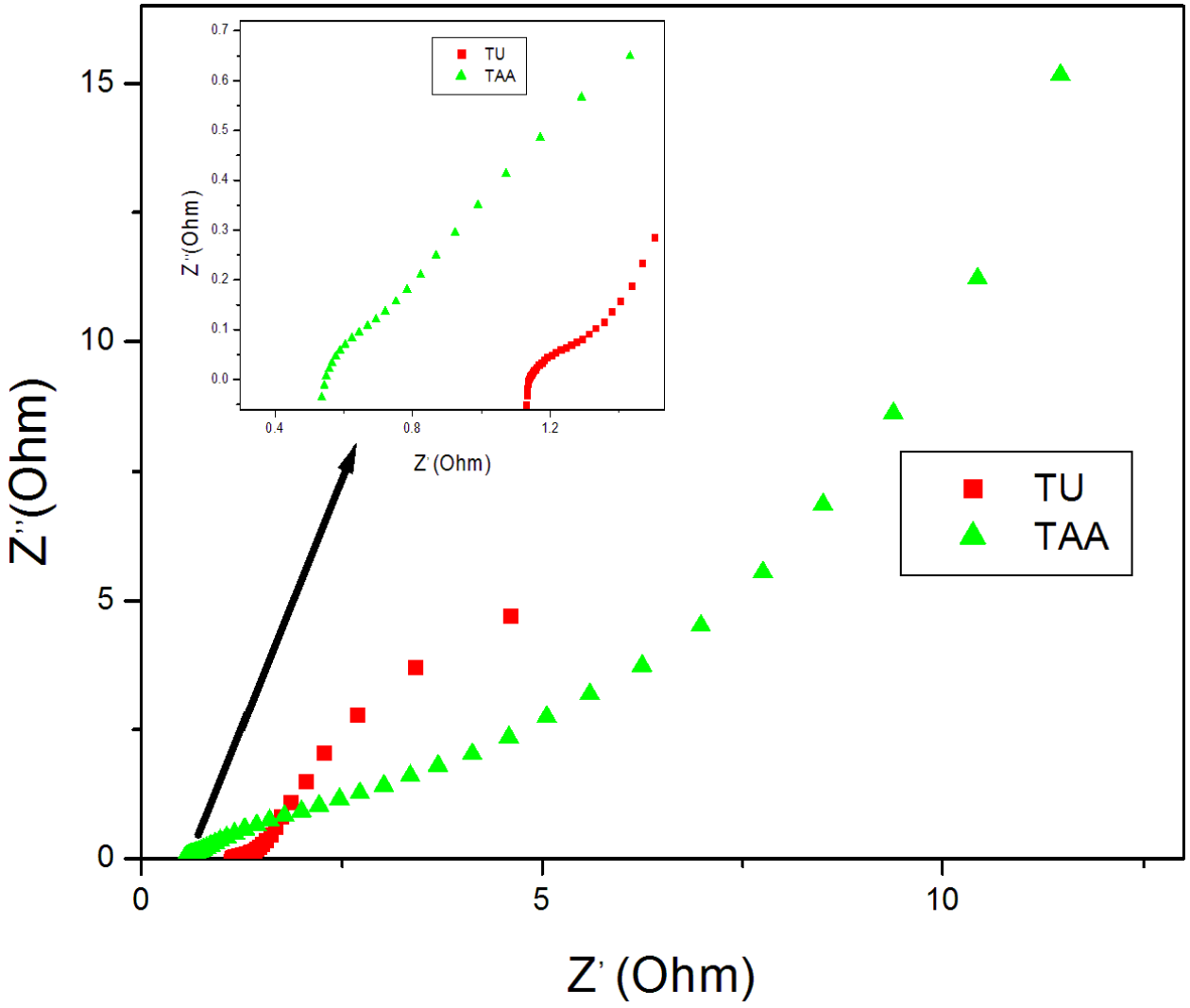
Z'' (Ohm)
Z' (Ohm)
TU
TAA
0
5
10
15
0
5
10
Z'' (Ohm)
Z' (Ohm)
TU
TAA
0.0
0.1
0.2
0.3
0.4
0.5
0.6
0.7
0.4
0.8
1.2

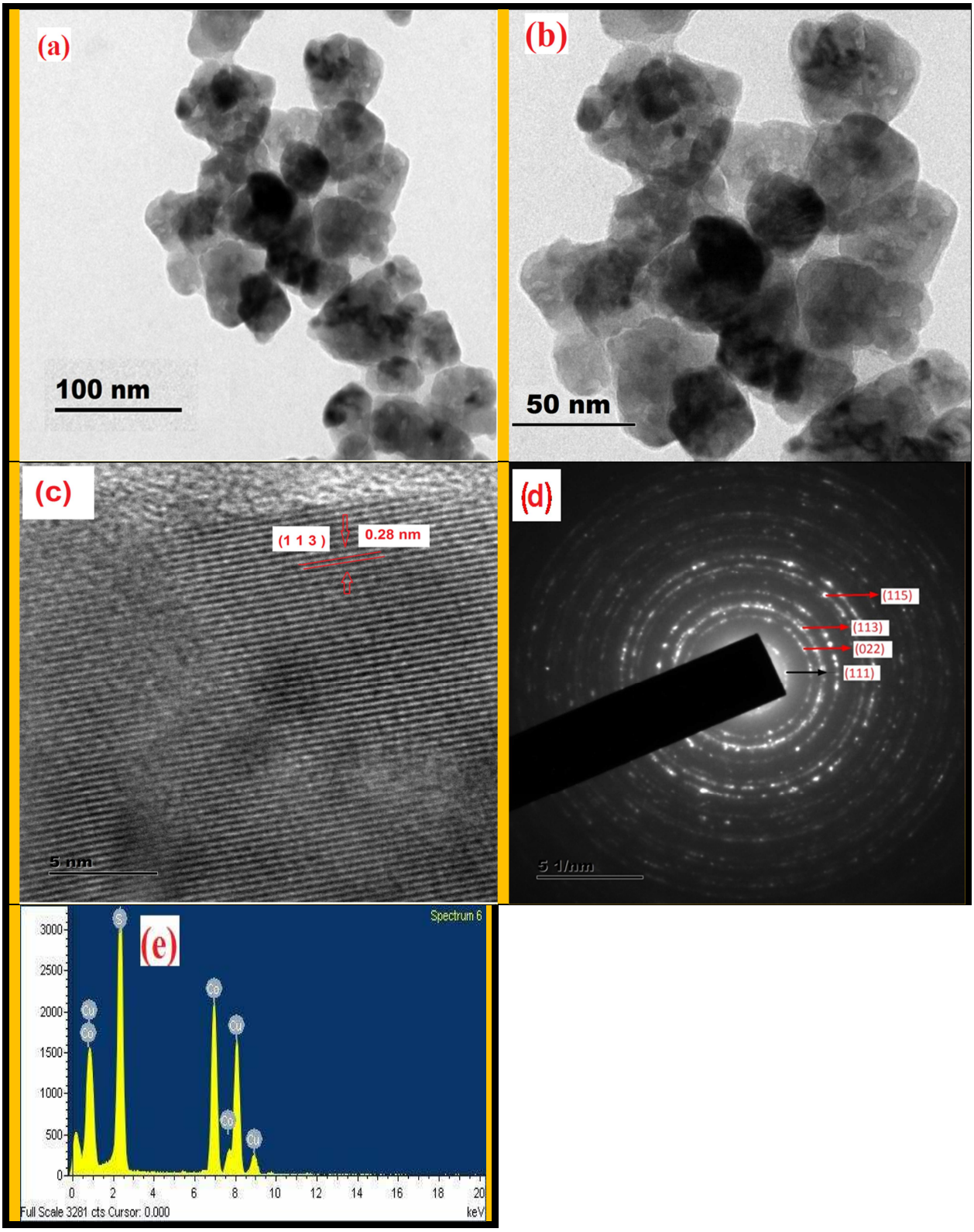
(a)
100 nm
(b)
50 nm
(c)
(1 1 3)
0.28 nm
5 nm
(d)
(115)
(113)
(022)
(111)
5 1/nm
(e)
Spectrum 6
Full Scale 3281 cts Cursor: 0.000
keV

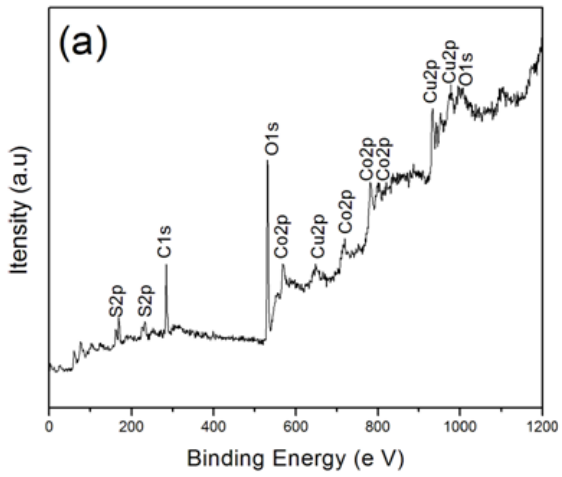
(a)
Itensity (a.u)
Binding Energy (e V)
S2p
S2p
C1s
O1s
Co2p
Cu2p
Co2p
Co2p
Co2p
Cu2p
Cu2p
O1s
0
200
400
600
800
1000
1200

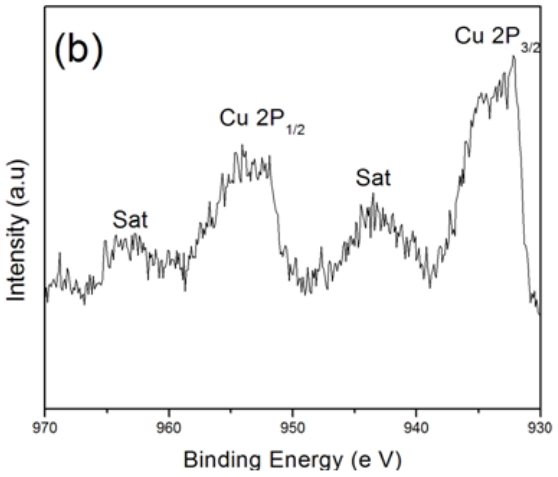
(b)
Intensity (a.u)
Binding Energy (e V)
Cu 2P3/2
Cu 2P1/2
Sat
Sat
970
960
950
940
930

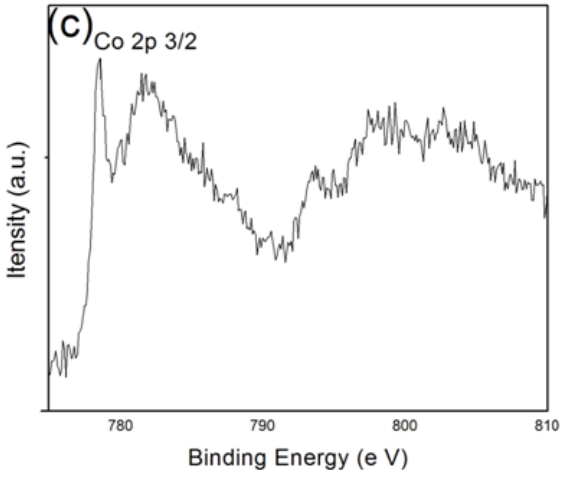
(c)
Co 2p 3/2
Itensity (a.u.)
Binding Energy (e V)
780
790
800
810

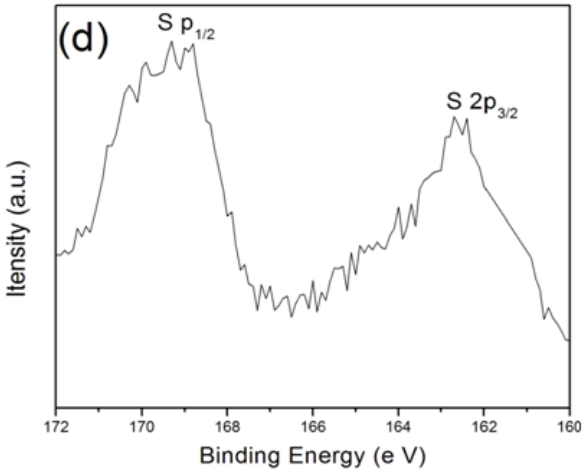
(d)
S p1/2
S 2p3/2
Itensity (a.u.)
Binding Energy (e V)
172
170
168
166
164
162
160

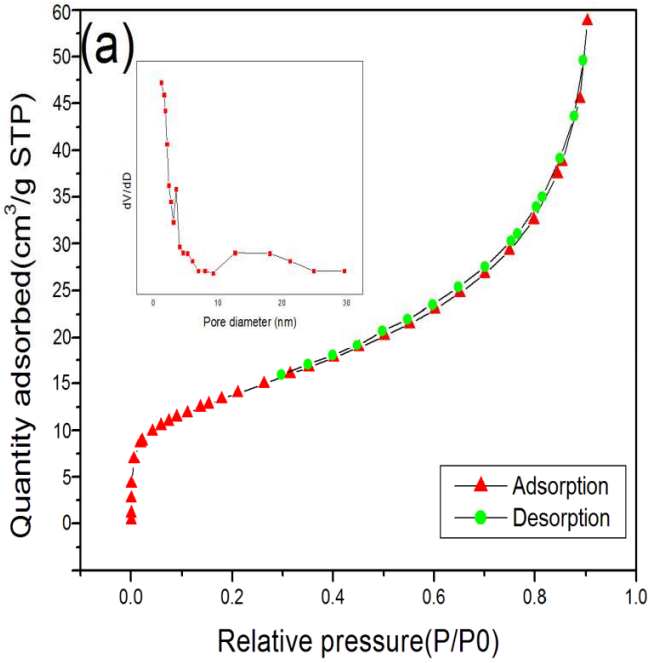
(a)
Quantity adsorbed(cm3/g STP)
Relative pressure(P/P0)
dV/dD
Pore diameter (nm)
Adsorption
Desorption

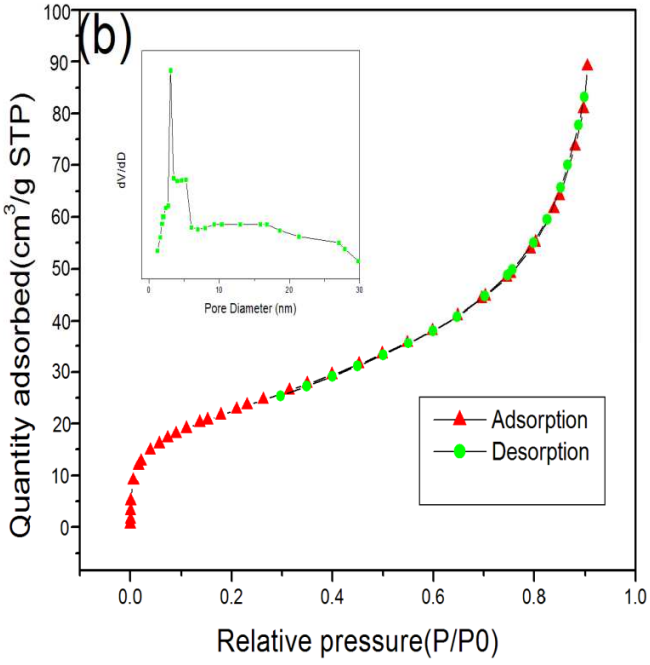
(b)
Quantity adsorbed(cm3/g STP)
Relative pressure(P/P0)
dV/dD
Pore Diameter (nm)
Adsorption
Desorption

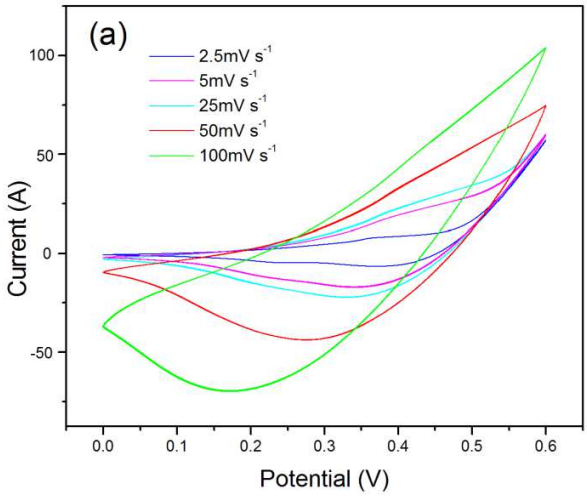
(a)
2.5mV s-1
5mV s-1
25mV s-1
50mV s-1
100mV s-1
Current (A)
Potential (V)

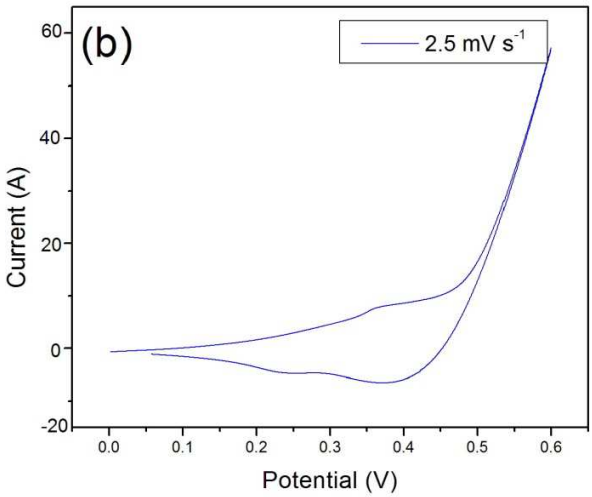
(b)
2.5 mV s-1
Current (A)
Potential (V)

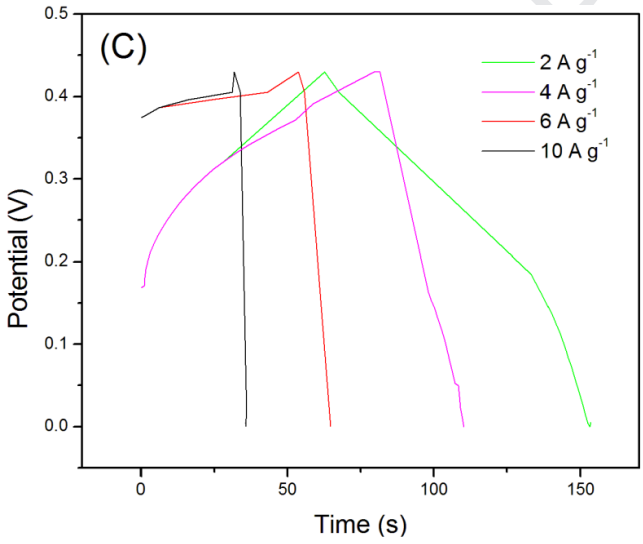
(C)
2 A g-1
4 A g-1
6 A g-1
10 A g-1
Potential (V)
Time (s)

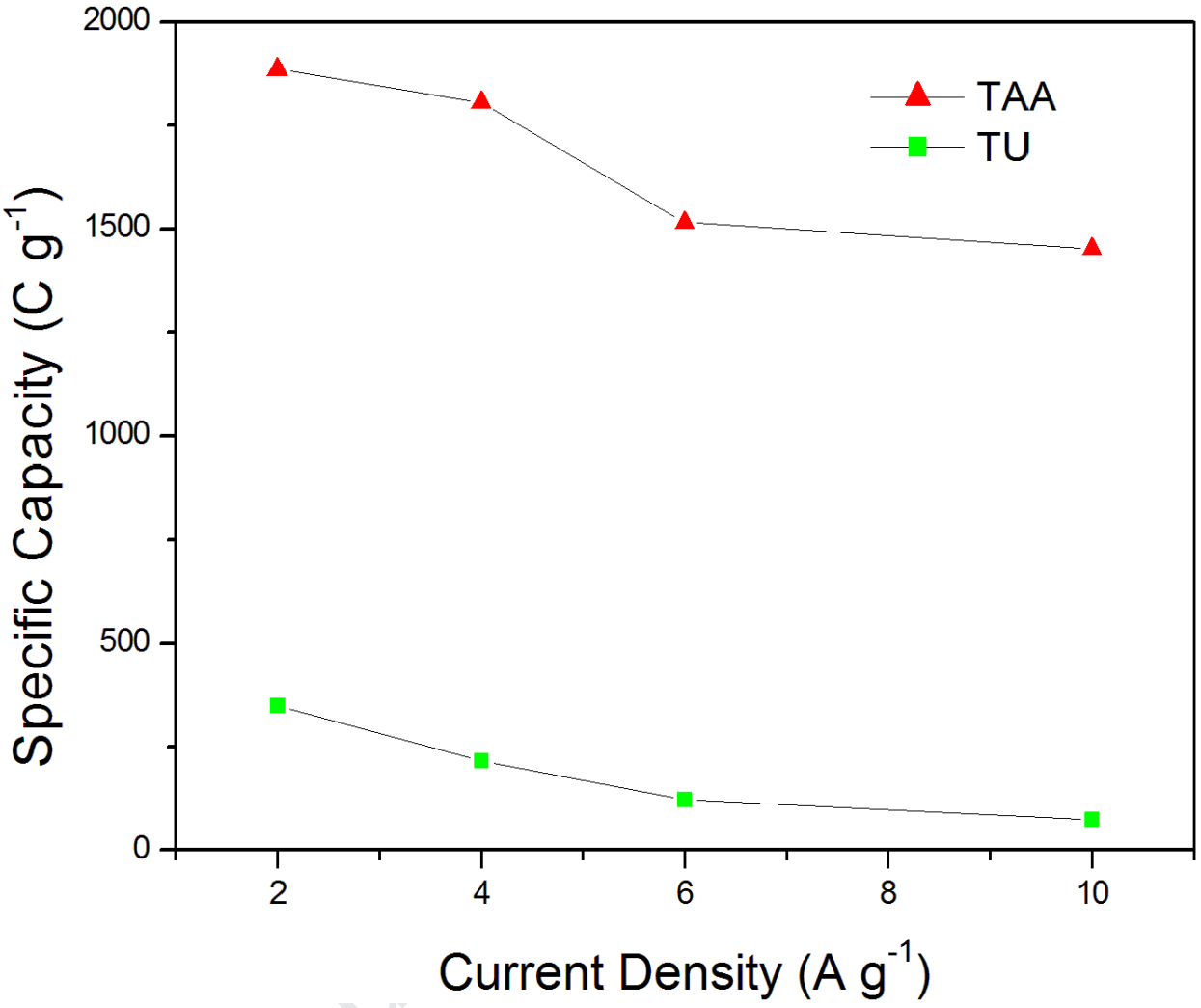
2000
1500
1000
500
0
2
4
6
8
10
Specific Capacity (C g-1)
Current Density (A g-1)
TAA
TU

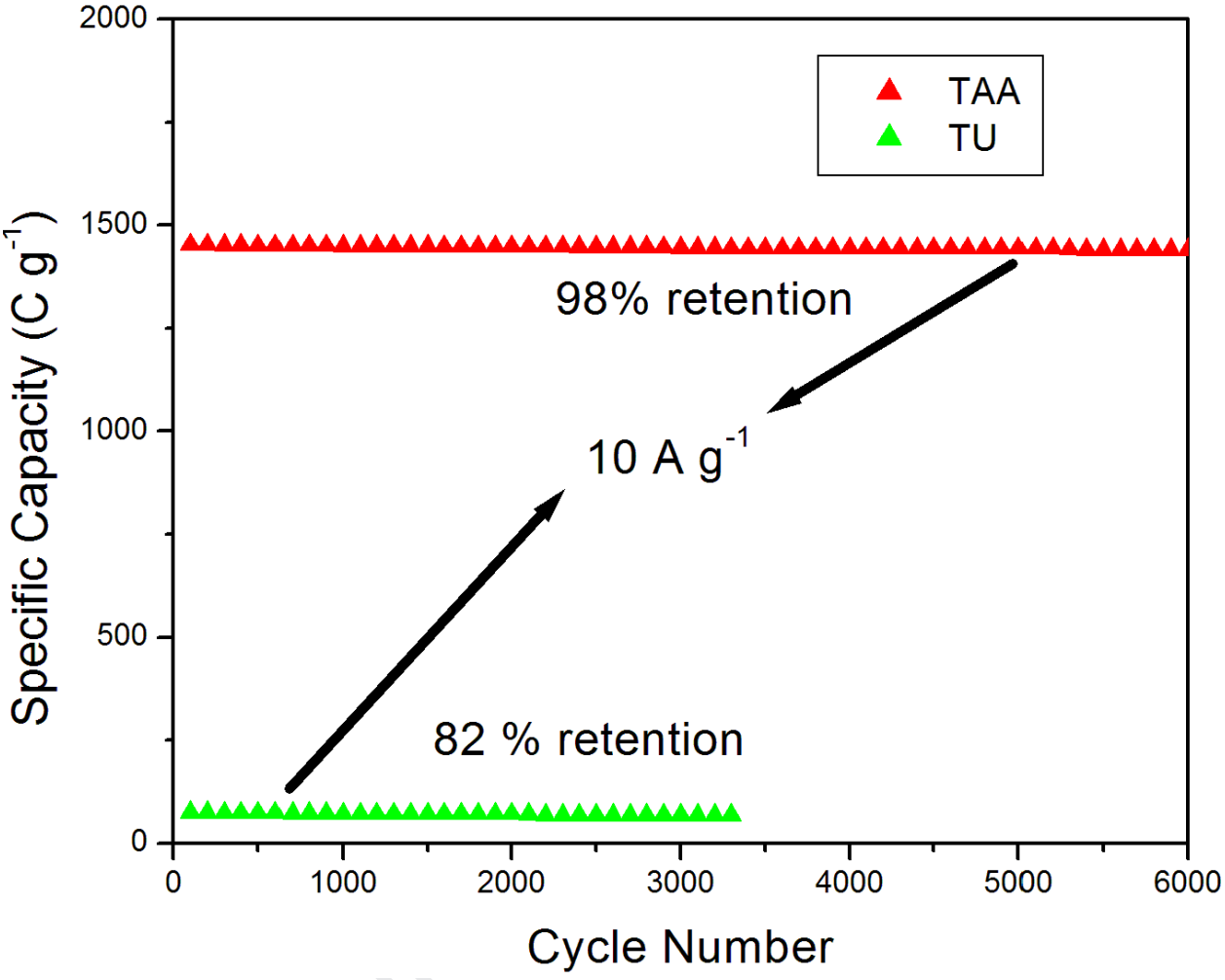
TAA
TU
98% retention
10 A g-1
82 % retention
Specific Capacity (C g-1)
Cycle Number
2000
1500
1000
500
0
0
1000
2000
3000
4000
5000
6000

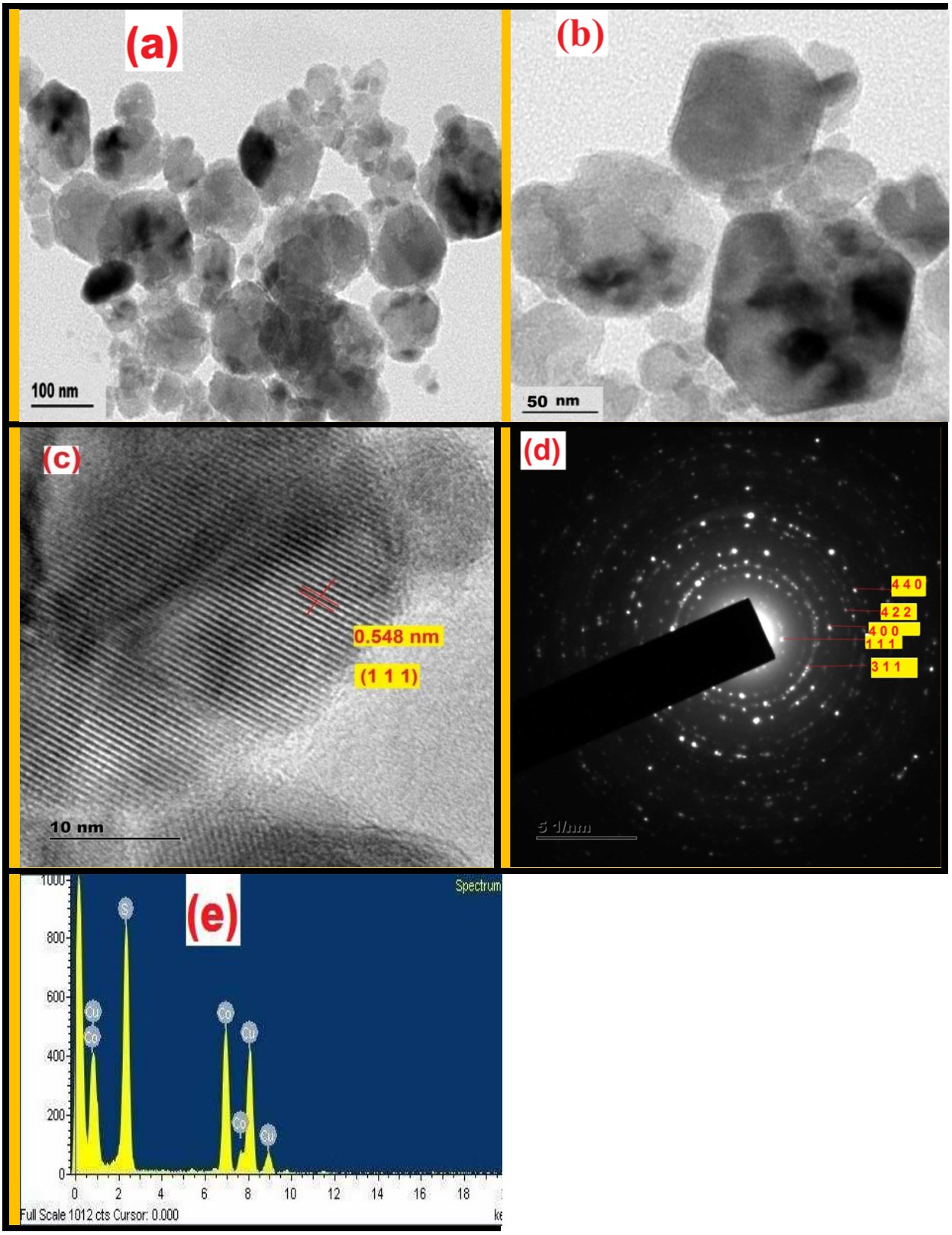
(a)
100 nm
(b)
50 nm
(c)
0.548 nm
(1 1 1)
10 nm
(d)
4 4 0
4 2 2
4 0 0
1 1 1
3 1 1
(e)
Spectrum
Cu
Co
S
Co
Cu
Co
Cu
Full Scale 1012 cts Cursor: 0.000

Highlights

- This paper reports the hydrothermal preparation of $CuCo_2S_4$ nanoparticles using two different sulfur sources
- They provide a high specific capacity of 523mAhg^{-1} at a current density of 2 A g^{-1} and excellent cyclic stability.
- They offer a high energy density of 41.89 W h kg^{-1} at a power density of 318.31W kg^{-1}.

Conflicts of interest

We declare that we do not have any commercial or associative interest that represents a conflict of interest in connection with the work submitted.